Falloff Curves for the Recombination Reaction Cl + FC(O)O + M → FC(O)OCl + M†

María P. Badenes, Adela E. Croce, and Carlos J. Cobos*,‡

Instituto de Investigaciones Fisicoquímicas Teóricas y Aplicadas (INIFTA), Departamento de Química, Facultad de Ciencias Exactas, Universidad Nacional de La Plata, CONICET, CICPBA, Casilla de Correo 16, Sucursal 4, (1900) La Plata, Argentina

Received: August 15, 2005; In Final Form: December 10, 2005

The pressure dependence of the recombination reaction Cl + FC(O)O + M → FC(O)OCl + M has been investigated at 296 K. FC(O)O radicals and Cl atoms were generated by laser flash photodissociation of FC(O)OO(O)CF at 193 nm in mixtures with Cl_2 and He or SF_6 over the total pressure range 8−645 Torr. The measured FC(O)O radical and F atom yields in the photolysis are 0.33 ± 0.06 and 0.67 ± 0.06. The reaction lies in the falloff range approaching the high-pressure limit. The extrapolations toward the limiting low- and high-pressure ranges were carried out using a reduced falloff curves formalism, which includes a recent implementation for the strong-collision broadening factors. The resulting values for the low-pressure rate coefficients are $(2.2 \pm 0.4) \times 10^{-28}$[He], $(4.9 \pm 0.9) \times 10^{-28}$[$SF_6$], $(1.9 \pm 0.3) \times 10^{-28}$[$Cl_2$] and $(5.9 \pm 1.1) \times 10^{-28}$[FC(O)OO(O)CF] cm^3 molecule^{-1} s^{-1}. The derived high-pressure rate coefficient is $(4.4 \pm 0.8) \times 10^{-11}$ cm^3 molecule^{-1} s^{-1}. For the reaction Cl + FC(O)OCl → Cl_2 + FC(O)O a rate coefficient of $(1.6 \pm 0.3) \times 10^{-11}$ cm^3 molecule^{-1} s^{-1} was determined. The high-pressure rate coefficient was theoretically interpreted using SACM/CT calculations on an ab initio electronic potential computed at the G3S level of theory. Standard heat of formation values of −99.9 and −102.5 kcal mol^{-1} were computed at the G3//B3LYP/6-311++G-(3df,3pd) level of theory for *cis*-FC(O)OCl and *trans*-FC(O)OCl, respectively. The computed electronic barrier for the conversion between the trans and cis conformers is 8.9 kcal mol^{-1}. On the basis of the present results, the above reactions are expected to have a negligible impact on stratospheric ozone levels.

1. Introduction

Simple unimolecular bond fission reactions and the reverse bond-forming recombination processes play essential roles in many practical environmental systems. For this reason, chemical kinetics compilations of a number of reactions relevant, for instance, in the combustion[1] and atmospheric[2,3] chemistry have been reported along the years. It is well-known that the initial linear dependence of the rate coefficients at low pressures is followed by a falloff transition region leading finally into the high-pressure regime characterized by a rate coefficient independent of both the nature and the pressure of the bath gas. From the microscopic point of view, the kinetic behavior of these processes is governed by a competition between collisional energy transfer, at the low-pressure limit, and intramolecular dynamics, at the high-pressure limit. At intermediate pressures both processes are simultaneously operative. In this context, the interplay and exchange of ideas between experimental and theoretical research provide an excellent testing ground for current unimolecular reaction theory. Therefore, an understanding of the factors that dominate these rate coefficients with the goal of making reliable predictions of unavailable experimental data appears highly desirable.

In this context, the recombination reaction between chlorine atoms and fluoroformyloxyl radicals, FC(O)O forming fluoroformyl hypofluorite

$$\mathrm{Cl + FC(O)O + M \rightarrow FC(O)OCl + M} \qquad (1)$$

is considered in the present study. After the earlier studies on the kinetics and the reaction mechanisms of FC(O)O and the related FCO and $FC(O)O_2$ radicals reactions, no direct kinetic experiments related to these species appeared until the end of the last century.[4−8] In fact, certainly motivated by the assumed potential atmospheric importance of these species in cycles of depletion of stratospheric ozone, several time-resolved studies mostly performed by the flash photolysis technique have appeared since the nineties.[9−26] In addition, several spectroscopic[27−34] and ab initio quantum chemical studies dealing with the molecular properties of the FCO_x ($x = 1-3$) radicals have been reported.[22−27,29,32,34,35−45]

The appearance of FC(O)O radicals in the atmosphere follows FCO and $FC(O)O_2$ successive formation. The FCO radical is likely to be generated by photolysis of CF_2O, and other carbonyl halides such as HFCO and CFClO, which are major degradation products of the photooxidation of fluorine containing halomethanes and haloethanes in the upper atmosphere.[46] The FCO is stable to dissociation, and its lifetime under stratospheric conditions long enough to allow collisions with other species that compete with photolysis. The FCO dominant loss process is the reaction with molecular oxygen to form $FC(O)O_2$ radicals. This reaction is also the major formation process of $FC(O)O_2$. The formation of FC(O)O in the last step of the aforementioned sequence of formation is accomplished by the reaction of $FC(O)O_2$ with NO. As for reaction 1, it has been invoked in one proposed ozone-regenerating cycle of the stratosphere and has been experimentally[20] and theoretically studied.[35,36] This process has been suggested to be of potential relevance in the isolation of chlorine atoms as stable FC(O)OCl. If so, it could be a chlorine reservoir species. In addition, ClO radicals eventually

† Part of the special issue "Jürgen Troe Festschrift".

‡ E-mail: cobos@inifta.unlp.edu.ar.

10.1021/jp054591x CCC: $33.50
Published on Web 02/04/2006

formed together with FCO radicals by photolysis of FC(O)OCl induced by solar light play a role in ClO catalytic cycles.

This Article is concerned with an experimental and theoretical investigation of the pressure dependence of reaction 1 at 296 K. Preliminary rate data for this process and for the Cl abstraction reaction from the FC(O)OCl formed in (1) by Cl atoms

$$Cl + FC(O)OCl \rightarrow Cl_2 + FC(O)O \qquad (2)$$

have been reported from this laboratory.[20] Expanding this study, the aim of the present investigation is to determine the limiting low-pressure, $k_{1,0}$, and high-pressure, $k_{1,\infty}$, rate coefficients from the experimental falloff curve. An approximate value of $k_{1,\infty} = (3.1 \pm 0.3) \times 10^{-11}$ cm^3 molecule^{-1} s^{-1} was obtained by averaging experiments carried out above 130 Torr total pressure.[20] In addition, a detailed theoretical investigation of the kinetics of reaction 1 based on a realistic ab initio electronic potential is reported in the present study.

2. Experimental Technique

The experimental technique has been described in detail elsewhere.[14,18,20,22−26] Therefore, only a brief description is presented here. The radicals FC(O)O were formed by 193 nm photodissociation of bis(fluoroformyl)peroxide, FC(O)OO(O)CF (5−40 Torr), in mixtures with Cl_2 (2−5 Torr) and the bath gases He (10−566 Torr) and SF_6 (5−638 Torr). The absence of slow, activated, processes prior to the photolysis pulse was checked by IR spectrophotometry of stabilized mixtures of Cl_2 and FC(O)OO(O)CF. Similarly to the behavior observed in the 366 nm photolysis of F_2 in mixtures with FC(O)OO(O)CF, no thermal reactions occur in the present mixture at all.[6]

An excimer laser (Lambda Physik, EMG 101 MSC) operating on the ArF transition was employed as a photolysis source. As discussed in section 3.1, under these conditions about 33% of FC(O)O radicals and 67% of F atoms are generated.[13] Afterward, F atoms react with Cl_2 according to reaction 3, $k_3 = 1.6 \times 10^{-10}$ cm^3 molecule^{-1} s^{-1},[47]

$$F + Cl_2 \rightarrow ClF + Cl \qquad (3)$$

Under the present conditions, the lifetime of the F atoms is less than 100 ns such that they are quantitatively converted into Cl atoms in less than 200 ns. Therefore, the reaction between F and FC(O)O radicals is unimportant within the present microsecond time scale.

The FC(O)O radical presents a visible absorption spectrum with origin at 760 nm (B $^2A_1 \leftarrow$ X $^2B_2$ transition) with an intense series of progressions superimposed on a broad background.[10,13,27] The wavelength of 545 nm, which lies in an almost unstructured region of the FC(O)O spectrum, has been selected for detection. Neither the related radicals FCO[9,12] nor the $FC(O)O_2$[10,12] absorb in the visible region. In fact, they have been detected at 300 and 240 nm, respectively, in the study of the FCO + $FC(O)O_2$ → 2 FC(O)O reaction.[22]

The FC(O)O temporal dependence was probed in real time with a spectral resolution of $\Delta\lambda = 1.1$ nm using a xenon high-pressure arc lamp (Hanovia, 150 W). A crossed beam geometry between the photolytic and the spectroscopic light beams was used in the present experiments. A cylindrical quartz cell of 5 cm diameter and 5 cm length was employed as a reaction vessel. The laser beam (0.8 cm high and 2.4 cm wide) traversed the cell through flat windows. Perpendicular to this, the analysis light (0.2 cm high and 0.9 cm wide) ran across the laser-flashed volume. The probed volume (0.4 cm^3) was located at the center of the laser beam volume (1.7 cm^3). Therefore, the analyzed volume is more than a factor of 4 smaller than the photolyzed one. For a typical FC(O)OO(O)CF pressure of 10 Torr the absorbed laser light at 0.9 cm is only of 14% of the incident on the mixture. Therefore, no significant concentration gradients of radicals from the interaction volume toward the walls of the vessel during the monitoring time were expected to occur. In fact, no appreciable deviations from the second-order kinetics behavior due to first-order diffusional processes have been observed at all. After passing the reaction quartz cell, the probe beam was directed onto the entrance slit of a prism monochromator (Zeiss, MM12), equipped with a photomultiplier tube (RCA, 1P28). Following amplification, the signal was monitored on a digital storage oscilloscope (LeCroy, 9310CM). Both the laser and the oscilloscope were synchronized with a digital delay generator (Stanford Research Systems, DG535). The absorption signals were subsequently stored in a computer. Laser pulse energies incident on the photolysis cell of typically 30 mJ cm^{-2} were measured with a calibrated pyroelectric detector (Gentec, ED-500) and the analysis beam intensity was recorded with a digital oscilloscope (Nicolet 2090). The experiments were performed at 296 K.

The gases were handled in a Pyrex vacuum system, and the pressure measured with a calibrated pressure transducer (MKS Baratron, 310CA) and with a sensitive quartz spiral gauge. FC(O)OO(O)CF was prepared by the thermal reaction of F_2 with CO in the presence of O_2 at 313 K, and purified by trap-to-trap distillations at low temperatures.[48,49] The other gases used had the following stated minimum purities: He, 99.999% (Union Carbide); F_2, 98% (Air Products); O_2, 99.9% (La Oxígena); CO, 99,9% (Matheson), SF_6, 99,999% (Matheson).

3. Results and Discussion

3.1. FC(O)O Yield in the FC(O)OO(O)CF Photolysis and Rate Coefficients for Reactions 1 and 2. FC(O)OO(O)CF exhibits a continuous UV absorption spectrum with an onset near 250 nm which increases in intensity up to at least 185 nm. At the photolysis wavelength of 193 nm, a measured absorption cross-section of 5.0×10^{-19} cm^2 molecule^{-1} has been reported.[50] Cl_2 presents a Gaussian absorption band with a maximum absorption cross-section of 2.55×10^{-19} cm^2 molecule^{-1} at 330 nm, which decreases to a much smaller value of 2.0×10^{-21} cm^2 molecule^{-1} at 260 nm such that no absorption at 193 nm is expected.[3] The product yield from FC(O)OO(O)CF photolysis at 193 nm has been determined at 233−353 K by three different methods.[13] In one of them, a F atom production at 295 K of $\Phi_F = 0.70 \pm 0.12$ was determined by comparison with an assumed unitary Cl atom yield in the 193 nm photolysis of CH_3Cl. Because the O−O bond (bond dissociation energy of 30.9 kcal mol^{-1} [22]) is certainly expected to be broken by the absorption of the 193 nm photon, by difference, $\Phi_{FC(O)O} = 0.30 \pm 0.12$ results. In a second method, the values $\Phi_F = 0.67 \pm 0.05$ and $\Phi_{FC(O)O} = 0.33 \pm 0.05$ were measured by monitoring in real time the $C_2H_5O_2$ concentrations generated in the photolysis of FC(O)OO(O)CF in the presence of C_2H_6 and O_2. Finally, the quantum yields were derived following the formed FNO after the irradiation of FC(O)OO(O)CF in mixtures with NO diluted in N_2. From these experiments, values of $\Phi_F = 0.71 \pm 0.03$ and $\Phi_{FC(O)O} = 0.29 \pm 0.03$ were determined. It is assumed that following the prompt FC(O)O−O(O)CF bond fission, a substantial concentration of highly vibrationally excited FC(O)O radicals are subsequently dissociated into F atoms and CO_2.[13] The experiments described below are quite consistent with these results.

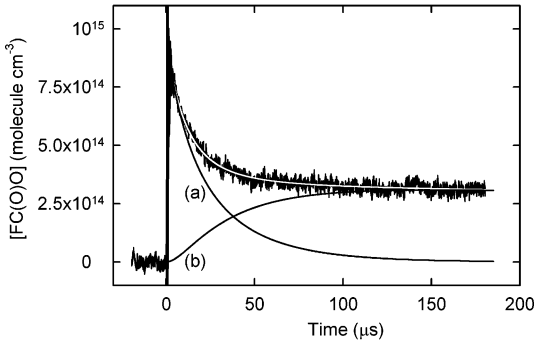

Figure 1. Time-resolved FC(O)O concentration detected at 545 nm following the 193 nm photodissociation of 10.0 Torr of FC(O)OO(O)CF in the presence of 5.3 Torr of Cl_2 and 151.4 Torr of He. The best fit was obtained with $k_1 = (3.0 \pm 0.5) \times 10^{-11}$ cm^3 molecule^{-1} s^{-1}, $k_2 = (1.5 \pm 0.3) \times 10^{-11}$ cm^3 molecule^{-1} s^{-1} and $\Phi_{FC(O)O} = 0.33 \pm 0.06$. The solid lines are the results of the modeling described in the text. (a) Individual contribution of reaction 1. (b) Individual contribution of reaction 2.

A typical signal showing the time-resolved FC(O)O concentration, [FC(O)O], recorded at 545 nm after the photolysis of 10.0 Torr of FC(O)OO(O)CF in the presence of 5.3 Torr of Cl_2 diluted in 151.4 Torr of He is depicted in Figure 1.

The FC(O)O concentrations were calculated from the detected absorbance signals and the absorption cross-section given in ref 10 after a reduction of about a 60% as recommended in ref 13, that is, $\sigma_{FC(O)O} = (2.8 \pm 0.3) \times 10^{-18}$ cm^2 molecule^{-1} at 545 nm. The observed decay is mostly attributed to reactions 1 and 2. Other possible reaction channels of reaction 1, would be Cl + FC(O)O → ClO + FCO and Cl + FC(O)O → ClF + CO_2. Using heat of formation values of +29.0, −90.7, +24.3 and −45.1 kcal mol^{-1} for Cl,[3] FC(O)O,[26] ClO[3] and FCO,[26] an endotermicity of 40.7 kcal mol^{-1} is estimated for the first reaction. For the second one, a four center transition state located 40.1 kcal mol^{-1} above the reagents Cl and FC(O)O is predicted by quantum chemical calculations performed at the PMP3/6-31G(2d) level. Therefore, these alternative pathways for reaction 1 are not operative.

The self-recombination of FC(O)O radicals completes the reaction scheme.

$$\text{FC(O)O} + \text{FC(O)O} + \text{M} \rightarrow \text{FC(O)OO(O)CF} + \text{M} \quad (4)$$

This process, important in the millisecond time scale, explains the slow subsequent decay observed in the absorption signals. A high-pressure rate coefficient of $(7.0 \pm 1.1) \times 10^{-13}$ cm^3 molecule^{-1} s^{-1} for reaction 4 has been determined by monitoring the FC(O)O at 545 by an experimental technique identical to the one employed here.[18] In another kinetic study a value $(5.5 \pm 0.6) \times 10^{-13}$ cm^3 molecule^{-1} s^{-1} measured at a total pressure of 217 Torr has been reported.[13] The contribution of other reaction channels of the FC(O)O self-reaction such as FC(O)O + FC(O)O → F(O)CC(O)F + O_2 or FC(O)O + FC(O)O → F_2 + $2CO_2$ can be ruled out on energetic grounds. In fact, employing an estimated F(O)C−C(O)F bond dissociation energy of 80.7 kcal mol^{-1} (PMP4/6-31G(d))[38] and the above heat of formation values for FCO and FC(O)O,[26] an enthalpy change of 10.1 kcal mol^{-1} is predicted for the first process. Although the second reaction is exothermic by 8.4 kcal mol^{-1}, it most likely does not operate on kinetic grounds. In fact, for the similar reaction FO_2 + FO_2 → F_2 + $2O_2$, an extremely small rate coefficient of 2.4×10^{-33} cm^3 molecule^{-1} s^{-1} has been measured.[51] On the other hand, both experimental and theoretical kinetic evidences suggest that reaction 4 is the exclusive reaction channel.[18]

If the FC(O)OO(O)CF pressure is changed over the range 5−40 Torr, similar k_2 values (see below) are recovered. This fact suggests that the reaction

$$\text{Cl} + \text{FC(O)OO(O)CF} \rightarrow \text{FC(O)OCl} + \text{FC(O)O} \quad (5)$$

is not operative. However, the similar process F + FC(O)OO(O)CF → FC(O)OF + FC(O)O (rate coefficient 1.5×10^{-15} cm^3 molecule^{-1} s^{-1} at 295 K) plays a role in the mechanism of the 193 nm photolysis of FC(O)OO(O)CF.[26]

The present experiments would not allow precluding the presence of the abstraction reaction

$$\text{FC(O)O} + \text{Cl}_2 \rightarrow \text{FC(O)OCl} + \text{Cl} \quad (6)$$

However, a large endothermicity of 17.0 kcal mol^{-1} is estimated for reaction 6. For this calculation we had employed the above heat of formation values for FC(O)O[26] and Cl[3] and the computed value of −102.5 kcal mol^{-1} for the *trans*-FC(O)OCl (section 3.3(b)). Therefore, reaction 6 is not expected to play any role. It should be noted that an activation energy of 16.2 kcal mol^{-1} (rate coefficient of 1.5×10^{-23} cm^3 molecule^{-1} s^{-1} at 298 K) has been measured for the similar reaction $FS(O_2)O + Cl_2 \rightarrow FS(O_2)OCl + Cl$.[52]

The pronounced initial FC(O)O decrease observed in Figure 1 is almost exclusively ascribed to reaction 1. Afterward, above 40 μs, the rate of FC(O)O consumption decreases strongly with time. This is interpreted considering the participation of reaction 2, which operates significantly when FC(O)OCl concentration increases because of reaction 1. As mentioned, the modeling of the absorption signals has been done by employing a whole mechanism formed by reactions 1−4. In the numerical simulations, we reproduce each experimental profile by fitting the rate coefficients k_1 and k_2, $\Phi_{FC(O)O}$ and the initial radical concentration $[FC(O)O]_0$. The Cl atom concentrations are given by $[Cl]_0 \approx [F]_0 = [FC(O)O]_0(1 - \Phi_{FC(O)O})/\Phi_{FC(O)O}$. The quality of a particular fit is shown in Figure 1. In addition, the individual contributions of reactions 1 and 2 to the signals are also indicated. The decay line (a) corresponds almost exclusively to the recombination reaction 1, whereas the contribution of reaction 3 is negligible. This behavior is similar to the experimental traces obtained in the 193 nm photolysis of FC(O)OO(O)CF, where the FC(O)O decay is mostly because of the reaction F + FC(O)O + M → FC(O)OF + M.[26] On the other hand, the growing line (b) corresponds to the FC(O)O concentration increase by reaction 2. At times much larger than those recorded in Figure 1, the decrease of FC(O)O concentration can be totally ascribed to reaction 4. The FC(O)O concentration vanishes near to 10 ms.[18]

The determined second-order rate coefficients for reactions 1 and 2 and the individual $\Phi_{FC(O)O}$ values are given in Table 1.

The listed errors arise from estimated signal noise of about 15% and from an uncertainty of 10% in $\sigma_{FC(O)O}$.[13] These sources of error are statistically independent, and therefore, the total errors were estimated as $\sigma = (\sum_i \sigma_i^2)^{1/2}$.

Because, under the present experimental conditions, reactions 3 and 4 have nanosecond and millisecond time scales, errors on the derived k_1 and k_2 values arisen from uncertainties in k_3 and k_4 are negligible. This fact is confirmed by modeling sensibility analysis. The resulting average value $\Phi_{FC(O)O} = 0.33 \pm 0.06$ agrees very well with the value measured in ref 13 of 0.31 ± 0.03.

For convenience, reaction 2 is discussed first. The obtained average k_2 is $k_2 = (1.6 \pm 0.3) \times 10^{-11}$ cm^3 molecule^{-1} s^{-1}.

TABLE 1: Rate Coefficients for Reactions 1 and 2 and FC(O)O Radical Yield from FC(O)OO(O)CF Photolysis at 193 nm

p(He), Torr	$p(SF_6)$, Torr	$p(Cl_2)$, Torr	p(FC(O)OO(O)CF), Torr	k_1, cm^3 molecule^{-1} s^{-1}	k_2, cm^3 molecule^{-1} s^{-1}	$\Phi_{FC(O)O}$
		2.6	5.1	$(1.6 \pm 0.3) \times 10^{-11}$	$(1.7 \pm 0.3) \times 10^{-11}$	0.34 ± 0.06
		5.2	10.3	$(2.0 \pm 0.4) \times 10^{-11}$	$(1.5 \pm 0.3) \times 10^{-11}$	0.33 ± 0.06
	5.1	5.2	9.7	$(2.8 \pm 0.5) \times 10^{-11}$	$(2.0 \pm 0.4) \times 10^{-11}$	0.36 ± 0.06
	7.4	2.0	5.4	$(2.0 \pm 0.4) \times 10^{-11}$	$(1.7 \pm 0.3) \times 10^{-11}$	0.34 ± 0.06
	11.2	5.2	9.7	$(2.8 \pm 0.5) \times 10^{-11}$	$(1.8 \pm 0.3) \times 10^{-11}$	0.34 ± 0.06
	17.4	5.2	9.7	$(2.5 \pm 0.5) \times 10^{-11}$	$(1.5 \pm 0.3) \times 10^{-11}$	0.33 ± 0.06
	637.9	2.6	5.1	$(3.3 \pm 0.6) \times 10^{-11}$	$(1.5 \pm 0.3) \times 10^{-11}$	0.33 ± 0.06
10.1		5.1	10.2	$(2.2 \pm 0.4) \times 10^{-11}$	$(1.5 \pm 0.3) \times 10^{-11}$	0.33 ± 0.06
20.4		5.1	10.2	$(2.3 \pm 0.4) \times 10^{-11}$	$(1.6 \pm 0.3) \times 10^{-11}$	0.33 ± 0.06
31.0		5.0	10.5	$(2.6 \pm 0.5) \times 10^{-11}$	$(1.5 \pm 0.3) \times 10^{-11}$	0.33 ± 0.06
51.5		5.0	10.5	$(2.7 \pm 0.5) \times 10^{-11}$	$(1.7 \pm 0.3) \times 10^{-11}$	0.33 ± 0.06
85.2		5.1	10.2	$(2.8 \pm 0.5) \times 10^{-11}$	$(1.5 \pm 0.3) \times 10^{-11}$	0.33 ± 0.06
101.2		5.0	10.5	$(2.9 \pm 0.5) \times 10^{-11}$	$(1.7 \pm 0.3) \times 10^{-11}$	0.33 ± 0.06
151.4		5.3	10.0	$(3.0 \pm 0.5) \times 10^{-11}$	$(1.5 \pm 0.3) \times 10^{-11}$	0.33 ± 0.06
205.3		5.3	10.0	$(2.9 \pm 0.5) \times 10^{-11}$	$(1.5 \pm 0.3) \times 10^{-11}$	0.33 ± 0.06
402.8		5.0	10.6	$(3.5 \pm 0.6) \times 10^{-11}$	$(1.4 \pm 0.3) \times 10^{-11}$	0.33 ± 0.06
566.0		5.2	40.4	$(3.5 \pm 0.6) \times 10^{-11}$	$(1.0 \pm 0.2) \times 10^{-11}$	0.36 ± 0.06

This value is virtually identical to the previously reported value of $(1.5 \pm 0.2) \times 10^{-11}$ cm^3 molecule^{-1} s^{-1}.[20] Further evidences for the formation of Cl_2 by the abstraction of Cl atoms from other hypochlorites by Cl have been reported. In fact, in the stationary photolysis of CF_3OCl and in the photolysis of Cl_2 in the presence of CF_3OCl, the reaction products CF_3OOCF_3 and Cl_2 are exclusively formed.[53] Similarly, large amounts of SF_5OOSF_5 and Cl_2 are generated by photolysis of SF_5OCl which yields Cl atoms.[54] More recently, the role that reaction Cl + $ClOClO_3 \rightarrow Cl_2 + ClO_4$ plays in the mechanism of the 366 nm photolysis of Cl_2 in the presence of $ClOClO_3$ has been demonstrated.[55] On an absolute basis, the present k_2 value may be compared with those measured for other selected Cl abstraction reactions, i.e., 1.2×10^{-11} cm^3 molecule^{-1} s^{-1} for Cl + $CF_3OCl \rightarrow Cl_2 + CF_3O$,[56] 1.0×10^{-11} cm^3 molecule^{-1} s^{-1} for Cl + $ClONO_2 \rightarrow Cl_2 + NO_3$,[3] and 2.0×10^{-11} cm^3 molecule^{-1} s^{-1} for Cl + FC(O)OCl → Cl_2 + FC(O)O.[57]

As Table 1 shows, the measured k_1 changes by a factor of about 2 over the total pressure range studied. An inspection of the listed values shows that, although close to the high-pressure limit, our rate coefficients still lie in the falloff regime between the third- and the second-order kinetics. To obtain the rate coefficients $k_{1,0}$ and $k_{1,\infty}$ from them, an extrapolation of the measured k_1 values is required.

3.2. Falloff Curves for Reaction 1. The appreciably high pressure of the precursor FC(O)OO(O)CF employed in the experiments, which is expected to be a very efficient collider in the stabilization of the energized adduct formed in reaction 1, precludes a straightforward analysis of the falloff curves. Thus, they were analyzed using an iterative procedure[26] which combines Troe's reduced falloff curves method[58] with calculated strong-collision low-pressure rate coefficients k_0^{SC}, which neglect weak-collision effects (section 3.4(a)).[58,59] In the first procedure, the measured rate coefficients were extrapolated to the limiting rate coefficients employing the reduced expression[58]

$$\frac{k}{k_\infty} = F^{LH}(k_0/k_\infty)\, F(k_0/k_\infty) \qquad \text{(I)}$$

The factor $F^{LH}(k_0/k_\infty) = k_0/k_\infty/(1 + k_0/k_\infty)$ is the result of the simple Lindemann−Hinshelwood mechanism. Here, $k_0 = \lim_{[M]\rightarrow 0} k([M])$ and $k_\infty = \lim_{[M]\rightarrow\infty} k([M])$ are pseudo-second-order rate coefficients. The broadening factor $F(k_0/k_\infty)$ accounts for corrections due to the energy and total angular momentum dependence of the excited species and for the multistep character of the energy transfer process assisted by collisions. This factor is represented by[58]

$$F(k_0/k_\infty) \approx F_{cent}^{\,1/\{1+[(\log(k_0/k_\infty))/N]^2\}} \qquad \text{(II)}$$

with $N \approx 0.75 - 1.27 \log F_{cent}$ where $F_{cent} = F(k_0/k_\infty{=}1)$ is the center broadening factor. In this way, the three quantities k_0, k_∞ and F_{cent} characterize the falloff curve. Constant values of $F_{cent} = 0.6$ and $N = 1$ or even an empirical fit of F_{cent} are frequently employed in low-temperature applications. However, a more reliable theoretical modeling should be considered to account for the finer details of the falloff curves and to compare the derived limiting rate coefficients with that from theory. In fact, the factor F_{cent} is certainly reaction-dependent. To this end, $F(k_0/k_\infty)$ is factorized into weak- and strong-collision contributions

$$F(k_0/k_\infty) \approx F^{WC}(k_0/k_\infty) F^{SC}(k_0/k_\infty) \qquad \text{(III)}$$

The importance of using realistic F_{cent}^{SC} factors has been recently emphasized by Troe.[60] Consequently, an approach that implicitly accounts for transitional modes and is based on the statistical adiabatic channel/classical trajectory (SACM/CT) calculations has been employed in the analysis of reaction 1.[61,62] The model has been recently generalized to be applied to recombination reactions at low temperatures.[63] The analysis based on the reaction HO + $NO_2 \rightarrow HONO_2$ leads to F_{cent}^{SC} values at 300 K of 0.63, 0.59, 0.53, 0.47 and 0.42, for reactions of the type atom + diatomic, atom + polyatomic, diatomic + diatomic, diatomic + polyatomic and polyatomic + polyatomic. These values combined with weak-collision contributions (see below) have been proposed to be used in the modeling of atmospheric processes.[2] In the framework of this model, the strong-collision broadening factor is given by

$$F^{SC}(k_0/k_\infty) = (1+x)\sum_{J=0}^{\infty}(2J+1)\int_{E_0(J)}^{\infty}\left(\frac{dE}{k_B T}\right)[F_\rho F_W/(xF_\rho + F_W)]\exp\left(-\frac{E}{k_B T}\right) \qquad \text{(IV)}$$

where $x = k_0/k_\infty$ and

$$F_\rho = \frac{\rho(E,J)}{\sum_{J=0}^{\infty}(2J+1)\int_{E_0(J)}^{\infty}\left(\frac{dE}{k_B T}\right)\rho(E,J)\exp\left(-\frac{E}{k_B T}\right)} \qquad \text{(V)}$$

$$F_W = \frac{W(E,J)}{\sum_{J=0}^{\infty}(2J+1)\int_{E_0(J)}^{\infty}\left(\frac{dE}{k_BT}\right)W(E,J)\exp\left(-\frac{E}{k_BT}\right)} \quad \text{(VI)}$$

Here $E_0(J)$ is the dissociation threshold energy as a function of the total angular momentum (quantum number J). These centrifugal barriers were computed using an accurate ab initio electronic potential (section 3.3(b)). The energy E- and J-resolved total number of open channels $W(E,J)$ accounts for contributions arisen from the transitional modes. Conserved modes are assumed unexcited. $W(E,J)$ is approached as

$$W(E,J) \approx w_{cap}(E,J)\, f_{rigid}(E,J)\, W(E,J)^{PST} \quad \text{(VII)}$$

$W(E,J)^{PST}$ is calculated by space phase theory with the analytical expressions given in ref 64. The capture probability $w_{cap}(E,J) \approx [1 - E_0(J)/E]^2$ accounts for centrifugal barrier effects and the rigidity factor $f_{rigid}(E,J) \approx f_{rigid}(J=0)[1 - E_0(J)/E]^2$ corrects $W(E,J)^{PST}$ by anisotropy effects of the potential energy surface.[65] The harmonic density of states $\rho(E,J)$ is evaluated using the Whitten−Rabinowitch method.[62] The relevant molecular data required to calculate $F_{cent}^{SC}(k_0/k_\infty)$ are given in section 3.3.

Figure 2a shows $F^{SC}(k_0/k_\infty)$ values calculated at 300 K for reaction 1. There is a small shift of the F_{cent}^{SC} from $x = 1$ to $x = 0.69$, i.e., from $\log x = 0$ to $\log x = -0.16$. The minimum of the curve lies for $F_{cent}^{SC} = 0.60$. This value is essentially the same as that derived on the basis of the $HONO_2$ system of 0.59.[63] In addition, it is similar to that estimated with the equation $F_{cent}^{SC} \approx S_K^{(-0.62\pm0.05)} \approx (1 + r/2)^{(-0.62\pm0.05)}$ (r is the total number of external rotational modes of the recombination species, 3 for reaction 1) of 0.57 ± 0.03.[63] This simple expression allows us to make a rough estimation of the additional broadening in the falloff curves arisen from the conserved modes contribution. In fact, using the vibrational frequencies for *trans*-FC(O)OCl of 1925, 1187, 996, 762, 647 and 450 cm^{-1} (see below) an increase in S_K of about $S_{cm} = \Sigma(h\nu_i/k_BT)[\exp(h\nu_i/k_BT) - 1]^{-1} = 0.6$ is estimated. Thus, assuming that even the above simple formulas apply, a 13% reduction of F_{cent}^{SC} is estimated. This value yields an increase of about 17% in the extrapolated $k_{1,\infty}$. It should be noted, however, that only a full numerical simulation with a combined system of transitional and conserved modes can provide reliable results. Thus, in the absence of such a detailed treatment, the value $F_{cent}^{SC} = 0.60$ was employed in the present study.

Following ref 63, a modified form of eq II was used to represent the numerical results of Figure 2a

$$F^{SC}(k_0/k_\infty) \approx F_{cent}^{SC\ 1/\{1+[(\log(k_0/k_\infty)+0.16)/N(k_0/k_\infty)]^2\}} \quad \text{(VIII)}$$

The very nice fit of the computed $F^{SC}(k_0/k_\infty)$ achieved by using eq IX with a $N(k_0/k_\infty)$ relationship similar to the one proposed in ref 63

$$N(k_0/k_\infty) = [(0.75 - 1.27\log F_{cent}^{SC})/1.02]\{1.347 - 0.5409\log(k_0/k_\infty) + 0.05924[\log(k_0/k_\infty)]^2\}(k_0/k_\infty)^{0.1762} \quad \text{(IX)}$$

is apparent in Figure 2a. The dependence of $N(k_0/k_\infty)$ with the reduced pressure scale k_0/k_∞ is illustrated in Figure 2b. Weak-collision effects are approximately introduced in the falloff curves using expressions similar to (VIII) and (IX) (omitting the superscript SC) and considering $F_{cent} \approx F_{cent}^{SC}F_{cent}^{WC}$ with $F_{cent}^{WC} \approx \beta_c^{0.14}$ where β_c is the weak-collision efficiency.[58] Therefore, $F_{cent} \approx 0.60\ \beta_c^{0.14}$ for the present case.

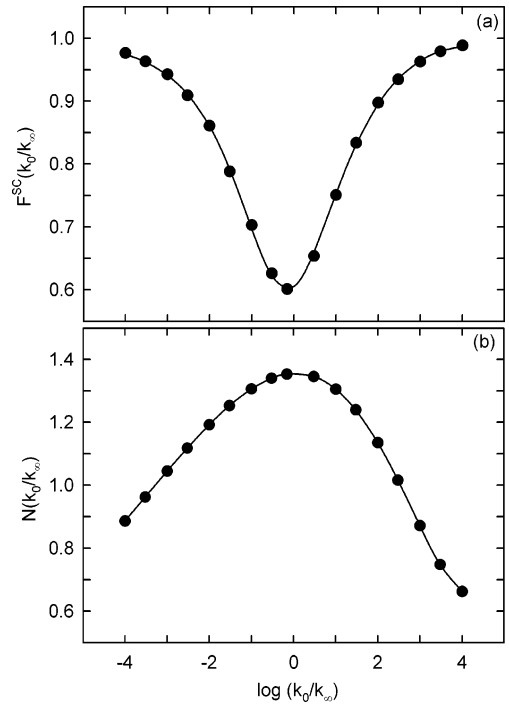

Figure 2. Strong-collision broadening factor (a) and width function (b) for reaction 1. (●) Calculated $F^{SC}(k_0/k_\infty)$ and $N(k_0/k_\infty)$ values. (a) Fit using eqs VIII and IX. (b) Fit using eq IX.

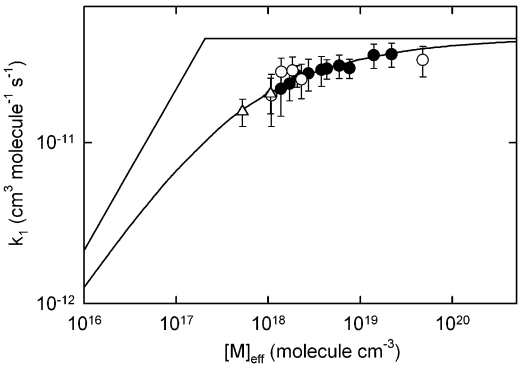

Figure 3. Falloff curve of the reaction 1. $[M]_{eff} = [He] + 2.30[SF_6] + 0.895[Cl_2] + 2.75[FC(O)OO(O)CF]$ (see text). Key: experiments with added He (●); experiments with added SF_6 (○); experiments without added bath gases (△). The solid line through the data is the fit with the Troe's formalism described in the text. The solid straight lines correspond to the limiting low- and high-pressure rate coefficients.

The k_1 values of Table 1 are depicted in Figure 3.

The effective third-body gas pressure relative to He, is given by

$$[M]_{eff} = [He] + [\beta_c(SF_6)\, Z_{LJ}(SF_6)/\beta_c(He)\, Z_{LJ}(He)][SF_6] + [\beta_c(Cl_2)\, Z_{LJ}(Cl_2)/\beta_c(He)\, Z_{LJ}(He)][Cl_2] + [\beta_c(FC(O)OO(O)CF)\, Z_{LJ}(FC(O)OO(O)CF)/\beta_c(He)\, Z_{LJ}(He)][FC(O)OO(O)CF] \quad \text{(X)}$$

Z_{LJ} are the Lennard-Jones collision frequencies between the excited adduct FC(O)OCl and the colliders. They were calculated using tabulated σ and ϵ/k_B parameters for He, Cl_2 and SF_6.[66] From estimated critical properties,[67] the values $\sigma = 4.7$ Å and $\epsilon/k_B = 264$ K for FC(O)OCl and $\sigma = 5.2$ Å and $\epsilon/k_B = 350$ K for FC(O)OO(O)CF were derived. The resulting Z_{LJ} values of 4.87×10^{-10}, 3.49×10^{-10}, 3.38×10^{-10} and 3.77

TABLE 2: Reaction Mechanism and Determined Rate Coefficients

reaction	rate coefficient, cm^3 $molecule^{-1}$ s^{-1}	ref
(1) Cl + FC(O)O + M → FC(O)OCl + M	$k_{1,0} = (2.2 \pm 0.4) \times 10^{-28}$[He]	this work
	$k_{1,0} = (4.9 \pm 0.9) \times 10^{-28}$[$SF_6$]	this work
	$k_{1,0} = (1.9 \pm 0.3) \times 10^{-28}$[$Cl_2$]	this work
	$k_{1,0} = (5.9 \pm 1.1) \times 10^{-28}$[FC(O)OO(O)CF]	this work
	$k_{1,\infty} = (4.4 \pm 0.8) \times 10^{-11}$	this work
(2) Cl + FC(O)OCl → FC(O)O + Cl_2	$(1.6 \pm 0.3) \times 10^{-11}$	this work
(3) F + Cl_2 → ClF + Cl	1.6×10^{-10}	47
(4) FC(O)O + FC(O)O → FC(O)OO(O)CF	$k_{4,\infty} = 7.0 \times 10^{-13}$	18

$\times 10^{-10}$ cm^3 $molecule^{-1}$ s^{-1} computed respectively for He, Cl_2, SF_6 and FC(O)OO(O)CF were then employed in the $[M]_{eff}$ estimation.

An analysis of the experimental falloff curve for M = He (Table 1) in terms of the above theoretical methodology was carried out. For this, a nonlinear fit of the k_1 vs $[M]_{eff}$ curve with the following trial set of collisional efficiencies: β_c(He) = 0.1, $\beta_c(Cl_2)$ = 0.4 and β_c(FC(O)OO(O)CF) = 0.6 was performed. This procedure delivered initial values for $k_{1,\infty}$ and $k_{1,0}$. The extrapolated $k_{1,0}$ was then confronted with the calculated strong-collision low-pressure rate coefficient $k_{1,0}^{SC}$(He) (defined as $k_{1,0} = \beta_c(He)k_0^{SC}(He)$[He] in section 3.4-(a)) to estimate a new β_c(He). Now fixing β_c(He) and the extrapolated $k_{1,\infty}$, $\beta_c(Cl_2)$ and β_c(FC(O)OO(O)CF) were fitted numerically together by a similar method. In this way, a new set of collision efficiencies for Cl_2 and FC(O)OO(O)CF were estimated. Repeating the above procedures until convergence, we obtained the final $k_{1,\infty}$, $k_{1,0}$(He), $k_{1,0}(Cl_2)$, $k_{1,0}$(FC(O)OO(O)CF), β_c(He), $\beta_c(Cl_2)$ and β_c(FC(O)OO(O)CF) values. It should be noted that if all the above parameters are simultaneously fitted, identical values are recovered for them. A similar strategy was employed to evaluate $k_{1,0}(SF_6)$ and $\beta_c(SF_6)$ employing for this case an initial $\beta_c(SF_6) = 0.6$ and the above determined $k_{1,\infty}$. The final collisional efficiencies for the gases He, SF_6, Cl_2 and FC(O)OO(O)CF are 0.14, 0.47, 0.18 and 0.51. Employing these and the above Z_{LJ} values in eq X we have $[M]_{eff} = [He] + 2.30[SF_6] + 0.895[Cl_2] + 2.75$[FC(O)OO(O)CF]. The effective pressure scale depicted in Figure 3 has been calculated with this expression. The obtained limiting rate coefficients are listed in Table 2. Errors due to uncertainties in the theoretical methods employed are difficult to quantify. However, the errors due the iterative numerical procedure fall well within the experimental limits. Therefore, they were not considered in the error bars which were estimated as above from the signal noise and $\sigma_{FC(O)O}$.[13]

The values corresponding to He and FC(O)OO(O)CF of 0.14 and 0.51 compare reasonably well with those reported for reaction F + FC(O)O + M → FC(O)OF + M of 0.10 and 0.55.[26] Other comparison with the present β_c values is provided by the results for the reaction F + $FS(O_2)O$ + M → $FS(O_2)OF$ + M.[68] For this process, values also consistent with the present of 0.11 and 0.50 were obtained for He and SF_6 respectively.

As Figure 3 shows, the results with added He are very well described by the fitted falloff curve. However, because of the larger scatter of the measurements, the agreement for M = SF_6 is just satisfactory. The bath gas concentration corresponding to the center of the falloff curve defined as $[He]_c = k_{1,\infty}/k_{1,0}$[He] is indicated in Figure 3 by the intersection of the two straight lines. In this way, the value $[He]_c = 2 \times 10^{17}$ molecule cm^{-3} (about 6 Torr) is obtained. By comparison, the center of the falloff curve for the recombination between F atoms and FC(O)O lies around 40 Torr He pressure.[26]

Our previous estimate of $k_{1,\infty} = 3.1 \times 10^{-11}$ cm^3 $molecule^{-1}$ s^{-1}, derived by averaging rate coefficients measured above 130 Torr total pressure,[20] is 25% smaller than the more accurate present value derived combining experimental and theoretical information provided by current unimolecular reaction rate models. At the highest gas density investigated the second-order rate coefficient is close to the 80% of the extrapolated $k_{1,\infty}$ value. The theoretical analysis of $k_{1,\infty}$ is discussed in section 3.4(b).

TABLE 3: Geometric Parameters for *cis*-FC(O)OCl and *trans*-FC(O)OCl (Bond Lengths in Angstroms, Angles in Degrees)

molecule	coordinate	B3LYP/ 6-311+G(3df)	HF/ 6-31G(2d)[a]
cis-FC(O)OCl	*r*(C−O)	1.345	1.327
	r(C═O)	1.178	1.157
	r(C−F)	1.325	1.291
	r(O−Cl)	1.712	1.671
	∠(O═CO)	121.6	129.4
	∠(FCO)	124.7	124.7
	∠(COCl)	119.1	115.0
	DIH(O═COCl)	180.0	180.0
trans-FC(O)OCl	*r*(C−O)	1.351	1.329
	r(C═O)	1.175	1.157
	r(C−F)	1.328	1.289
	r(O−Cl)	1.698	1.675
	∠(O═CO)	125.1	122.1
	∠(FCO)	130.4	124.3
	∠(COCl)	113.9	119.3
	DIH(O═COCl)	0.0	0.0

[a] Reference 35.

3.3. Quantum Chemical Calculations of FC(O)OCl Molecular Properties. *(a) Molecular Structures and Harmonic Vibrational Frequencies.* No experimental data of any property of FC(O)OCl are available. Therefore, the input data relevant for the kinetic analysis described in section 3.4 have been estimated as follows. To calculate fully optimized molecular structures and harmonic vibrational frequencies, we use the popular hybrid B3LYP density functional, which employs the Becke's three parameter exchange functional[69,70] coupled to the nonlocal correlational functional of Lee, Yang and Parr.[71] The large 6-311+G(3df) Pople's basis set was selected for all cases. These properties were calculated using respectively analytical gradient and analytical second derivative methods. The obtained molecular parameters for both isomers of FC(O)OCl together with reported estimations at the HF/6-31G(2d) level[35] are listed in Table 3.

The general agreement between both sets of calculations is satisfactory. However, the present more accurate results were used to estimate the rotational constants. The resulting values for the cis and trans conformers are $A = 0.377$, $B = 0.090$ and $C = 0.073$ cm^{-1} and $A = 0.384$, $B = 0.087$ and $C = 0.071$ cm^{-1}, respectively. Calculated harmonic vibrational frequencies, infrared intensities and approximate mode assignations are given in Table 4.

The mode assignments were obtained from the animation of the normal modes. Most of them are significantly mixed, and thus the consigned assignations are only approximate. For the

TABLE 4: Harmonic Vibrational Frequencies (in cm^{-1}), Mode Description and Infrared Intensities (in km mol^{-1}) for *cis*-FC(O)OCl and *trans*-FC(O)OCl

		B3LYP/6-311+G(3df)		HF/6-31G(2d)[a]	
molecule	mode description	frequencies	intensities	frequencies	intensities
cis-FC(O)OCl	C═O stretch	1908	459	1908	541
	C−O stretch	1218	419	1286	716
	C−F stretch	945	42	1021	35
	Cl−O stretch	753	10	826	18
	C out of plane	753	30	770	66
	FC═O bend	624	8	650	8
	OC═O bend	473	1	448	6
	COCl bend	248	0.3	244	5
	torsion	115	0.1	143	1
trans-FC(O)OCl	C═O stretch	1925	406	1919	706
	C−O stretch	1187	549	1278	594
	C−F stretch	996	34	1005	71
	Cl−O stretch	798	11	787	16
	C out of plane	762	29	760	67
	FC═O bend	647	3	618	9
	FCO bend	450	4	478	7
	COCl bend	245	4	251	1
	torsion	155	0.1	92	0

[a] Reference 35.

TABLE 5: Calculated Heats of Formation (in kcal mol^{-1}) for *cis*-FC(O)OCl, *trans*-FC(O)OCl from Atomization Energies[a]

level of theory	*cis*-FC(O)OCl	*trans*-FC(O)OCl
B3LYP/6-311+G(3df)	−98.9 (−98.0)	−100.6 (−99.6)
G3B3	−100.9 (−100.0)	−103.6 (−102.6)
G3//B3LYP/6-311+G(3df)	−101.0 (−100.1)	−103.6 (−102.6)

[a] Data in brackets correspond to 0 K.

sake of comparison, potential energy distribution calculations of the similar molecule FC(O)OF indicate that only the C═O stretching, the C out of plane and the torsion motions are decoupled from the rest of the modes.[72]

(b) Energetics. Heat of formation values for FC(O)OCl were computed also using the B3LYP/6-311+G(3df) method (including diffuse and extended polarization functions on hydrogen atoms when required) and, at a higher level of theory, using the G3B3 ab initio model chemistry.[73] A modified version G3//B3LYP/6-311+G(3df) that uses B3LYP/6-311+G(3df) calculations instead of B3LYP/6-31G(d) to estimate the geometry and the vibrational frequencies (without scaling) was also employed.[74] Under certain assumptions about additivity in the Gaussian-3 theory, the final energies are comparable to those computed at the high-level QCISD(T, full)/G3Large. This model accounts for spin−orbit, core and high-level empirical corrections. Two methods were employed to estimate the heats of formation. First, we derive the heats of formation at 0 K, $\Delta_{f,0}H°$ by subtracting the computed total atomization energies from the experimental heats of formation of the fluorine (18.47 ± 0.07 kcal mol^{-1}), chlorine (28.59 ± 0.001 kcal mol^{-1}), carbon (169.98 ± 0.1 kcal mol^{-1}) and oxygen atoms (58.99 ± 0.02 kcal mol^{-1}).[75] These values are then transformed to 298 K, $\Delta_{f,298}H$, using estimated thermal contributions and $H°$(298.15 K) − $H°$(0 K) values for fluorine, chlorine, carbon and oxygen atoms of 1.05, 1.10, 0.25 and 1.04 kcal mol^{-1}.[76] The resulting thermodynamic values computed for both isomers of FC(O)OCl are listed in Table 5.

A comparison with more accurate Gaussian-3 data shows that the B3LYP functional combined with extended 6-311+G(3df) basis set gives satisfactory results.

The employed second method normally leads to more accurate heats of formation values. This method relies on the selection of isodesmic (and isogyric) reaction schemes. In this type of reactions, systematic errors due to electron correlation energy and incompleteness of the basis sets (truncation in the one-electron basis set) almost cancel.[77] The strategy followed to compute $\Delta_{f,298}H$ for the molecule of interest consists of combining the computed enthalpy change of the selected reaction with well-established heats of formation of the rest molecules. The isodesmic reactions, the calculated enthalpy changes, Δ_rH, and the resulting $\Delta_{f,298}H$ values at different levels of theory are presented in Table 6.

In these calculations we use the following experimental heats of formation: (in kcal mol^{-1}): −17.9 (HOCl), −25.98 (H_2CO), −48.04 (CH_3OH), −56.8 (CH_3F), −17.80 (CH_4), −57.798 (H_2O), −145.3 (F_2CO), −19.4 (Cl_2O).[3] It should be noted that although the Δ_rH values for the different reactions are quite different, the derived $\Delta_{f,298}H$ values are certainly very close. In addition, the very good agreement between the values derived from atomization and isodesmic methods is apparent. All calculations indicate that trans structure is a global minimum. At the best level employed, G3//B3LYP/6-311+G(3df), the enthalpy difference between both rotomers at 298 K is of 2.6 kcal mol^{-1}. A similar value of 2.5 kcal mol^{-1} has been previously derived by UMP3/6-31G(2d) calculations.[35] By comparison, for FC(O)OF an energy gap of 1.2 kcal mol^{-1} has been reported.[72]

The theoretical kinetic analysis requires the knowledge of the internal rotational motions. The present estimated barrier for the trans → cis conversion is V_0 = 8.9 kcal mol^{-1}, which is similar to the experimental value for FC(O)OF of 9.7 kcal mol^{-1}.[50] The associated reduced moment of inertia estimated as $I_r = V_0/(8\pi^2\nu_{tors}^2)$, where ν_{tors} = 155 cm^{-1} is the torsional frequency, is 2.28 amu Å^2. The transition state is characterized by a low imaginary vibrational frequency of 123i cm^{-1} indicating a rather narrow rotational barrier.

The energetic along the minimum energy pathway of a recombination reaction plays a central role on kinetic models. The shape and the deepness of the electronic isotropic potential characterize fine rotational effects affecting these processes from the low- to the high-pressure limiting regions of the falloff curve. For this reason we have computed the radial potential of reaction 1 by ab initio quantum chemical methods. First, we compute the potential by using the G3//B3LYP/6-311+G(3df) model chemistry. The results for *trans*-FC(O)OCl illustrated in Figure

TABLE 6: Isodesmic Reactions, Calculated Enthalpy Changes and Heats of Formation (in kcal mol^{-1}) for *trans*-FC(O)OCl[a]

	B3LYP/6-311++G(3df,3pd)		G3B3		G3//B3LYP/6-311++G(3df,3pd)	
reaction	ΔH_r	$\Delta_{f,298}H$	ΔH_r	$\Delta_{f,298}H$	ΔH_r	$\Delta_{f,298}H$
$HOCl + H_2CO + CH_3OH + CH_3F \rightarrow FC(O)OCl + 2\,CH_4 + H_2O$	−45.9	−101.2	−48.0	−103.3	−47.8	−103.1
$HOCl + F_2CO + CH_3OH \rightarrow FC(O)OCl + CH_3F + H_2O$	−5.9	−102.6	−6.8	−103.4	−6.2	−102.9
$Cl_2O + 2F_2CO + 2CH_3OH \rightarrow 2FC(O)OCl + 2CH_3F + H_2O$	−9.4	*−101.0*	−10.4	*−103.1*	−10.4	*−101.6*
		−101.6		−103.3		−102.5
		(−100.6)		(−102.3)		(−101.5)
		−99.9		*−100.6*		*−99.9*
		(−99.0)		*(−99.7)*		*(−99.0)*

[a] Average data, in brackets, correspond to 0 K. The values in italics correspond to *cis*-FC(O)OCl.

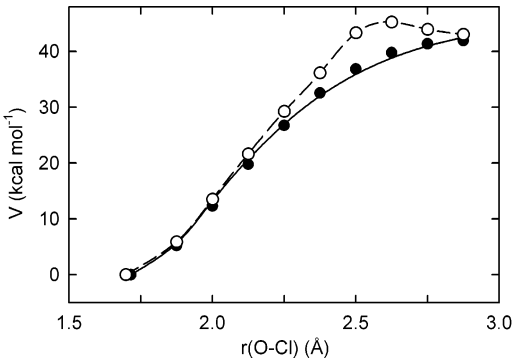

Figure 4. Potential energy curves for *trans*-FC(O)OCl → FC(O)O + Cl calculated at the G3//B3LYP/6-311+G(3df) (○) and G3S (l) levels. The straight line is a fit using the eq XI. The dashed line corresponds to a spline fit.

4 clearly indicate that this model predicts a small barrier located at a FC(O)O−Cl bond distance near to 2.6 Å. This potential is inconsistent with the present experimental high-pressure rate coefficients. Improved G3S ab initio calculations that correct for deficiencies in the G3 model at large elongations where transitional states are located were also performed.[78] This model is quite appropriate to compute minimum energy pathways for reactions, as the present, in which the reactants and products have a different number of electron pairs. In contrast to the G3 model, in the G3S, the high-level correction term (named HLC) depends on geometry and, thus, varies along the potential energy surface. The G3S approaches very well single-point QCISD-(T,full)/G3Large results on MP2(full)/6-31G(d) geometries. An overall accuracy near 1 kcal mol^{-1} is for the G3S model is estimated.[78] Figure 4 shows the G3S potential (in kcal mol^{-1}) and a fit performed with the Morse function

$$V(r) = 46.6\{1 - \exp[-2.678(r - 1.716)]\}^2 \qquad \text{(XI)}$$

A better fit can be certainly achieved by using, for instance, an *r*-dependent Morse parameter. However, we use the standard Morse potential, which is consistent with the SACM/CT calculations detailed in section 3.4. The extrapolated bond dissociation energy of 46.6 kcal mol^{-1} compares very well with the value of $D_e = \Delta_0 H° + \Delta ZPE = 45.3$ kcal mol^{-1}, obtained from the present $\Delta_{f,0}H°$ of −101.5 kcal mol^{-1} for *trans*-FC-(O)OCl and the values +28.59 and −87.2 kcal mol^{-1} for Cl[3] and FC(O)O,[26] and the vibrational zero-point energies of 10.2 and 7.8 kcal mol^{-1} for *trans*-FC(O)OCl and FC(O)O.[26] It is interesting to note that the computed $\Delta_0 H° = 42.9$ kcal mol^{-1} is identical to the value recently obtained for the O−Cl bond dissociation energy at 0 K of $FS(O_2)OCl$[57] and similar to the values in $ClOClO_2$, 39.6 kcal mol^{-1}, and $ClOClO_3$, 45.8 kcal mol^{-1}.[74]

These calculations also provide the effective rotational constants $B_{eff}(r) = [B(r) + C(r)]/2$ (in cm^{-1}) along the reaction coordinate. The computed values are very well reproduced with the expression

$$B_{eff}(r) = 0.0785/[1 + 0.3424(r - 1.716) + 0.1560(r - 1.716)^2] \qquad \text{(XII)}$$

All described calculations were carried out with the default integration grid of the Gaussian 03 program package employed.[79]

3.4. Theoretical Kinetic Analysis of the Low- and High-Pressure Rate Coefficients of Reaction 1. *(a) Low-Pressure Rate Coefficients.* At the low-pressure limit, the steady-state rate coefficient can be represented by the product of the collision efficiency β_c and the strong-collision rate coefficient k_0^{SC}.[59] The first depends on intermolecular energy transfer properties whereas the second one is characterized by the equilibrium populations of metastable molecular configurations. The largely employed Troe's factorized form

$$k_0 = \beta_c[M]Z_{LJ}\frac{\rho_{vib,h}(E_0)k_BT}{Q_{vib}}\exp\left(-\frac{E_0}{k_BT}\right)F_{anh}F_EF_{rot}F_{rot\ int}F_{Ez}\left(\frac{1}{K_C}\right) \qquad \text{(XIII)}$$

has been used in this study.[58,59] The significance and the values of the various factors in eq XIII are given in the following. The values for the Lennard-Jones collision frequencies Z_{LJ} were given in section 3.2. $\rho_{vib,h}(E_0) = 4.93 \times 10^5$ (kcal mol^{-1})$^{-1}$ is the harmonic vibrational density of states of *trans*-FC(O)OCl at the threshold energy $E_0 \approx \Delta_0 H° = 42.9$ kcal mol^{-1} and $Q_{vib} = 1.78$ the vibrational partition function of *trans*-FC(O)OCl. The *F* factors take into account corrections for anharmonicity ($F_{anh} = 1.21$), spread of internal energies ($F_E = 1.10$), external rotations ($F_{rot} = 17.07$), internal rotations ($F_{rot\ int} = 6.71$) and zero-point barrier ($F_{Ez} \approx 1$) effects. Finally, $K_C = k_{-1}/k_1 = 1.34 \times 10^{-7}$ cm^3 molecule^{-1} is the equilibrium constant evaluated with the molecular properties of *trans*-FC(O)OCl and FC(O)O.[26] To compute F_{rot}, the $E_0(J)$ values were derived from the maxima of the potential $V_{cent}(r) = V(r) + B_{eff}(r)(J(J+1))$ with $V(r)$ and $B_{eff}(r)$ given by eqs XI an XII, respectively. The centrifugal barriers were very well represented as $E_0(J) \approx C_\nu$-$[J(J+1)]^\nu$ when the parameters $C_\nu = 7.78 \times 10^{-3}$ cm^{-1} and $\nu = 1.13$ are used. Expressions for the different factors in eq XIV have been given elsewhere.[58,59]

The resulting k_0^{SC} for the different gases are 1.50×10^{-27}[He], 1.04×10^{-27}[SF_6], 1.08×10^{-27}[Cl_2], and 1.16×10^{-27}[FC(O)OO(O)CF] cm^3 molecule^{-1} s^{-1}. These values were employed to estimate β_c in the falloff analysis of section 3.2. Finally, following the simple expression which connects β_c with the average energy transferred in all up and down transitions (for an exponential collision model), $-\langle\Delta E\rangle \approx F_E k_B T\beta_c/(1 - \beta_c^{1/2})$,[80] we roughly estimate $-\langle\Delta E\rangle$ values of 52, 342, 70, 396

cm^{-1} for He, SF_6, Cl_2 and FC(O)OO(O)CF. Assuming an uncertainty of at least a factor of 2 in these numbers, they appear to be reasonable when compared to those measured in direct experiments of collisional energy transfer of highly excited molecules.[81] On the basis that $-\langle\Delta E\rangle$ remains almost constant between 200 and 400 K, we estimate the expression $k_{1,0} = 2.0 \times 10^{-28}(T/300)^{-2.7}$[He] cm^3 $molecule^{-1}$ s^{-1}.

It seems interesting at this time to compare the measured low-pressure rate coefficients against those obtained for the association reaction between F atoms and FC(O)O radicals.[26] The reported values for this reaction, $(1.6 \pm 0.3) \times 10^{-29}$[He] and $(7.1 \pm 1.5) \times 10^{-29}$[FC(O)OO(O)CF] cm^3 $molecule^{-1}$ s^{-1} are, on average, a factor of 11 smaller than the values listed in Table 2. This difference can be mostly attributed to the 5 times smaller harmonic vibrational density of states of *trans*-FC(O)OF ($\rho_{vib,h}$-(E_0 = 34.7 kcal mol^{-1}) = 9.78×10^4 (kcal $mol^{-1})^{-1}$ [26]) as compared with that corresponding to *trans*-FC(O)OCl. An additional factor of 2 results from the contribution of the total rotational degrees of freedom ($F_{rot}F_{rot\ int} \approx 56$ for *trans*-FC-(O)OF[26] and about 115 for *trans*-FC(O)OCl). Both effects altogether account for a factor of 10. The other terms in expression XIII almost cancel. This analysis explains the similarity in the collisional efficiencies derived for these reactions mentioned in section 3.2.

(b) High-Pressure Rate Coefficients. The above G3S calculations performed along the minimum energy pathway of reaction 1 revealed an energy profile without a maximum. Therefore, a smooth transition between some vibrational motions and separated fragment rotations is expected. An appropriate way to treat a reaction with such a potential at the high-pressure limit is provided by the SACM. This model allows to factorize the limiting high-pressure rate coefficient as $k_\infty = f_{rigid}k_\infty^{PST}$.[82,83] Here k_∞^{PST} denotes the rate coefficient for phase space theory derived with the isotropic part of the potencial[84,85] and f_{rigid} is the thermal rigidity factor which accounts for anisotropy.[83] For the calculation of k_∞^{PST} eq XIV applies

$$k_\infty^{PST} = f_{el}(k_B T/h)(h^2/2\pi\mu k_B T)^{3/2} Q_{cent}^* \qquad \text{(XIV)}$$

where the centrifugal partition function Q_{cent}^* is approached as

$$Q_{cent}^* = \Gamma(1 + 1/\nu)(k_B T/C_\nu)^{1/\nu} \qquad \text{(XV)}$$

For the present reaction, the electronic degeneracy factor is $f_{el} = Q_{el,FC(O)OCl}/Q_{el,Cl}Q_{el,FC(O)O} = 0.124$. The resulting value of $k_{1,\infty}^{PST} = 6.13 \times 10^{-11}$ cm^3 $molecule^{-1}$ s^{-1} suggests that anisotropic forces play only a minor role in reaction 1. In fact, the comparison of this value with the experimental, leads to an apparent experimental rigidity factor of $f_{rigid} \approx 0.72$. This value is between those estimated, by an identical treatment, for the association reactions F + FC(O)O, 0.36,[26] and Cl + $FS(O_2)O$, 0.90.[57]

The above value for f_{rigid} can be confronted with predictions based on the SACM/CT.[86] In this treatment, the dynamics of a valence interaction between an atom and a linear rotor is computed with a combination of classical trajectory (CT) and statistical adiabatic channel model (SACM) calculations on a Morse potential. Consequently, we approach the FC(O)O radical as a quasi-linear rotor with the molecular C_{2v} symmetry axis assimilated to a $C_{\infty v}$ axis of the linear rotor. Following the SACM/CT, for the low-temperature range one has

$$f_{rigid}(T\rightarrow 0) \approx (1 + Z^2 + Z^8)^{-1/8} \qquad \text{(XVI)}$$

where

$$Z = (C/3\sin^2\gamma_e)^n/\gamma_1 \qquad \text{(XVII)}$$

and

$$C = [\epsilon(r_e)]^2/2BD_e \qquad \text{(XVII)}$$

Here n and γ_1 are parameters that depend on the angle of the potential minimum γ_e, $\epsilon(r_e)$ is the adduct vibrational frequency of the transitional mode at the equilibrium bond length r_e and B the rotational constant of the fragment. For reaction 1, we employ $\gamma_e = 38.2°$ as estimated from the calculated *trans*-FC-(O)OCl structure, $D_e = 45.3$ kcal mol^{-1} and $B = 0.293$ cm^{-1}.[26] B3LYP/6-311+G(3df) calculations carried out along the reaction coordinate of *trans*-FC(O)O−Cl dissociation indicate that only the COCl bend (245 cm^{-1}) and torsion (155 cm^{-1}) modes decay strongly when the O−Cl bond increases. Therefore, the geometrical mean $\epsilon(r_e) = 195$ cm^{-1} was used in eq XVIII. To characterize the potential energy surface, we assume in principle a standard value of $\alpha/\beta = 0.5$ for the ratio between the anisotropy α and Morse parameters.[83] Using calculated values of $n = 0.386$, $\gamma_1 = 0.909$ and $C = 4.08$, the low-temperature rigidity factor $f_{rigid}(T\rightarrow 0) \approx 0.56$ results. The transformation of this value to 296 K was done using a center-of-mass value for the Morse parameter of 3.16 $Å^{-1}$. In this way, following the treatment of ref 86, the value $f_{rigid} \approx 0.53$ is derived. This SACM/CT value is 26% lower than the experimental of 0.72. An increased parameter of $\alpha/\beta = 0.62$ was used to match both values. Under this conditions, a small temperature dependence, typical for this type of reactions, of $k_{1,\infty} = 4.4 \times 10^{-11}(T/300)^{0.26}$ cm^3 $molecule^{-1}$ s^{-1} is obtained between 200 and 400 K.

It should be noted that the present SACM/CT rigidity factor of 0.53 compares reasonably well with that derived in ref 20 with a simplified SACM[82,83] of 0.35. In the latter a somewhat smaller parameter of $\alpha/\beta = 0.46$ was selected to fit the experimental $k_{1,\infty}$. On the other hand, both SACM versions lead to similar temperature dependencies of about $T^{0.3}$. Finally, a comparison between the high-pressure rate coefficients for the recombination reactions of F and Cl atoms with FC(O)O in terms of the above factorized expression $k_\infty = f_{rigid}k_\infty^{PST}$ [83] is presented. The modeling of both reactions is based on accurate G3S computations of their isotropic potentials which led to similar k_∞^{PST} values (5.9×10^{-11} cm^3 $molecule^{-1}$ s^{-1} for F + FC(O)O → FC(O)OF). Therefore, according to this analysis, the 2.1 times larger high-pressure rate constant measured for reaction 1 can be attributed to the larger f_{rigid} value for reaction 1 ($f_{rigid} \approx 0.36$ for F + FC(O)O → FC(O)OF) suggesting that anisotropy effects arising from the angular forces in the transitional modes play a smaller role for reaction 1.

3.5. Implications for Atmospheric Chemistry. On the basis of the derived room-temperature limiting rate coefficients for reaction 1 and the respective temperature dependences here estimated, the atmospheric implications of this process will be briefly considered following the analysis of ref 13. For this, a room-temperature value of $k_{1,0} \approx 2 \times 10^{-28}$[air] cm^3 $molecule^{-1}$ s^{-1} similar to that measured for He and Cl_2 is assumed. The analysis is performed at altitudes near 40 km, where the FC-(O)O concentration is probably more significant. At this altitude, the temperature and the total density are close to 250 K and 1×10^{17} molecule cm^3, respectively.[3] Under these conditions a second-order rate coefficient of about 1×10^{-11} cm^3 $molecule^{-1}$ s^{-1} is estimated by employing a temperature independent center broadening factor of 0.5. Taking into account that the tropospheric background FC(O)O concentration is surely much

smaller than that corresponding to Cl of 6×10^5 molecule cm^3, the pseudo-first-order loss rate for FC(O)O with respect to the reaction with Cl atoms is calculated. The resulting lifetime for FC(O)O is 2×10^3 min. This value is notably larger than those reported for the reactions of FC(O)O with the NO, NO_2, O_3 and HO_2 molecules of 0.5, 4, 5 and 80 min, respectively.[13] Therefore, reaction 1 is expected to be unimportant in the atmosphere. In addition, the photodissociation of FC(O)O into F atoms and CO_2 could decrease significantly atmospheric concentration of FC(O)O. Certainly, assuming a unitary quantum yield over the whole absorption band, the calculated FC(O)O atmospheric photolysis frequency at 40 km is 0.29 s^{-1}.[17] These facts preclude the participation of reaction 1 in ozone-regenerating cycles of the stratosphere.[35,36]

4. Summary and Conclusions

The knowledge of the kinetics of the recombination reaction processes is of major importance. In addition to the kinetics information itself, the studies of this type of reaction, which involve the formation of a simple bond, provide a special searching test for theories of unimolecular reactions and relevant parts of ab initio potential energy surfaces. a study of the 193 nm laser flash photolysis of FC(O)OOC(O)F in the presence of Cl_2 and He or SF_6 at 296 K has been presented here. These experiments allow to study for a first time the pressure dependence of the recombination reaction Cl + FC(O)O + M → FC(O)OCl + M. The experimental results have been combined with a detailed modeling of the measured falloff curves with different Troe's formulations of statistical unimolecular rate theory. For this, recent strategies for the strong-collision broadening factors for barrierless reactions at low temperatures[63] have been applied to the present reaction. The treatment accounts for contributions of centrifugal barriers, angular momentum coupling and anisotropy effects of the potential energy surface.[65,86] The analysis also accounts for weak-collision effects through the Troe's factorized formalism for the low-pressure rate coefficients.[58,59,80] From this combined method the value $(4.4 \pm 0.8) \times 10^{-11}$ cm^3 molecule^{-1} s^{-1} for the high-pressure rate coefficient, and the values $(2.2 \pm 0.4) \times 10^{-28}$[He], $(4.9 \pm 0.9) \times 10^{-28}$[$SF_6$], $(1.9 \pm 0.3) \times 10^{-28}$[$Cl_2$] and $(5.9 \pm 1.1) \times 10^{-28}$[FC(O)OO(O)CF] cm^3 molecule^{-1} s^{-1} for the low-pressure rate coefficients have been determined. As expected, the present $k_{1,\infty}$ value is somewhat larger than the previously derived on the basis of more limited high-pressure information.[20] From the low-pressure rate coefficients measured for the gases He, SF_6, Cl_2 and FC(O)OO(O)CF, the collision efficiencies 0.14, 0.47, 0.18 and 0.51 were estimated. The obtained values for the gases He and FC(O)OO(O)CF compare nicely with those derived for the similar reaction F + FC(O)O + M → FC(O)OF + M of 0.10 and 0.55.[26] For the reaction Cl + FC(O)OCl → FC(O)O + Cl_2 a reaction rate coefficient of $(1.6 \pm 0.3) \times 10^{-11}$ cm^3 molecule^{-1} s^{-1} was measured in excellent agreement with our preliminary results.[20]

In the absence of experimental data, molecular parameters for FC(O)OCl, were estimated by using the density functional theory at the B3LYP/6-311+G(3df) level. In this way, reliable molecular structures and harmonic vibrational frequencies of the cis and trans conformers of FC(O)OCl were obtained. The respective heat of formation values at 298 K were determined from enthalpies computed for selected isodesmic reactions at the high G3//B3LYP/6-311+G(3df) level. The resulting values for the cis and trans conformers are −99.9 and −102.5 kcal mol^{-1}, being the electronic barrier that separates them of 8.9 kcal mol^{-1}.

A high-level G3S electronic potential for the FC(O)O−Cl bond breaking was used in all our kinetic calculations. This potential allowed us to estimate the accurate centrifugal barriers used in the falloff curve calculations, in the evaluation of the rotational factors of the low-pressure rate coefficients and in the phase space high-pressure rate coefficients.

The internally consistent analysis presented here for reaction 1 allowed us to obtain very good fits of the experimental falloff curves. The interplay between experiments and theory is obligatory for a complete understanding of the details of the falloff curves. In the present paper we illustrate a methodology to derive realistic extrapolations to the limiting rate coefficients. The measured values allow quantifying the relevance of this process in atmospheric chemistry. A simple analysis indicates that both reactions 1 and 2 are unimportant for the atmospheric modeling.

Acknowledgment. This research project was supported by the Universidad Nacional de La Plata, the Consejo Nacional de Investigaciones Científicas y Técnicas (CONICET) (PIP 0450), the Comisión de Investigaciones Científicas de la Provincia de Buenos Aires (CICPBA), the Agencia Nacional de Promoción Científica y Tecnológica (PICT 06-06786), the Fundación Antorchas and the Max Planck Institute for Biophysical Chemistry Göttingen through the "Partner Group for Chlorofluorocarbons in the Atmosphere". A.E.C. and C.J.C. thank to Professor Jürgen Troe for continuing support and hospitality.

References and Notes

(1) Baulch, D. L.; Bowman, C. T.; Cobos, C. J.; Cox, R. A.; Just, Th.; Kerr, J. A.; Pilling, M. J.; Stocker, D.; Troe, J.; Tsang, W.; Walker, J.; Warnatz, J. *J. Phys. Chem. Ref. Data* **2005**, *34*, 757.

(2) Atkinson, R.; Baulch, D. L.; Cox, R. A.; Crowley, J. N.; Hampson, R. F.; Hynes, R. G.; Jenkin, M. E.; Rossi, M. J.; Troe, J. *Atmos. Chem, Phys.* **2004,** *4*, 1461. See also http://www.iupac-kinetic.ch.com.ac.uk/.

(3) Sander, S. P.; Friedl, R. R.; Golden, D. M.; Kurylo, M. J.; Huie, R. E.; Orkin, V. L.; Moortgat, G. K.; Ravishankara, A. R.; Kolb, C. E.; Molina, M. J.; Finlayson-Pitts, B. J. *Chemical Kinetics and Photochemical Data for Use in Atmosferic Studies*; NASA/JPL Data Evaluation, JPL Publication 02-25 Evaluation No. 14; NASA: Pasadena, CA, February 2003. (See http://jpldataeval.jpl.nasa.gov/.)

(4) Heras, J. M.; Arvia, A. J.; Aymonino, P. J.; Schumacher, H. J. *Z. Phys. Chem. NF* **1961**, *28*, 250.

(5) Arvia, A. J.; Aymonino, P. J.; Schumacher, H. J. *Z. Phys. Chem. NF* **1966**, *51*, 170.

(6) Croce, A. E.; Tori, C. A.; Castellano, E. *Z. Physik. Chem. NF* **1989**, *162*, 161.

(7) Croce, A. E.; Castellano, E. *Z. Phys. Chem. NF*, **1994**, *185*, 165.

(8) Croce, A. E.; Tori, C. A.; Castellano, E. *Z. Phys. Chem. NF* **2002**, *216*, 947.

(9) Maricq, M. M.; Szente, J. J.; Khitrov, G. A.; Francisco, J. S. *Chem. Phys. Lett.* **1992**, *199*, 71.

(10) Maricq, M. M.; Szente, J. J.; Khitrov, G. A.; Francisco, J. S. *J. Chem. Phys.* **1993**, *98*, 9522.

(11) Behr, P.; Goldbach, K.; Heydtmann, H. *Int. J. Chem. Kinet.* **1993**, *25*, 957.

(12) Wallington, T. J.; Ellermann, T.; Nielsen, O. J.; Sehested, J. *J. Phys. Chem.* **1994**, *98*, 2346.

(13) Maricq, M. M.; Szente, J. J.; Dibble, T. S.; Francisco, J. S. *J. Phys. Chem.* **1994**, *98*, 12294.

(14) Cobos, C. J.; Croce, A. E.; Castellano, E. *Chem. Phys. Lett.* **1995**, *239*, 320.

(15) Behr, P.; Shafranovsky, E.; Heydtmann, H. *Chem. Phys. Lett.* **1995**, *247*, 327.

(16) Wallington, T. J.; Schneider, W. F.; Mogelberg, T. E.; Nielsen, O. J.; Sehested, J. *Int. J. Chem. Kinet.* **1995**, *27*, 391.

(17) Mörs, V.; Argüello, G. A.; Hoffmann, A.; Malms, W.; Röth, E. P.; Zellner, R. *J. Phys. Chem.* **1995**, *99*, 15899.

(18) Croce, A. E.; Cobos, C. J.; Castellano, E. *Chem. Phys.* **1996**, *211*, 215.

(19) Behr, P.; Heydtmann, H. *Ber. Bunsen-Ges. Phys. Chem.* **1996**, *100*, 553.

(20) Cobos, C. J.; Croce, A. E.; Castellano, E. *Chem. Phys. Lett.* **1997**, *266*, 253.
(21) Behr, P.; Kaupert, C.; Shafranovski, E.; Heydtmann, H. *Int. J. Chem. Kinet.* **1998**, *30*, 329.
(22) Badenes, M. P.; Castellano, E.; Cobos, C. J.; Croce, A. E.; Tucceri, M. E. *Chem. Phys. Lett.* **1999**, *303*, 482.
(23) Badenes, M. P.; Castellano, E.; Cobos, C. J.; Croce, A. E.; Tucceri, M. E. *Chem. Phys.* **2000**, *253*, 205.
(24) Tucceri, M. E.; Badenes, M. P.; Croce, A. E.; Cobos, C. J. *Chem. Commun.* **2001**, 71.
(25) Tucceri, M. E.; Badenes, M. P.; Croce, A. E.; Cobos, C. J. *Phys. Chem. Chem. Phys.* **2001**, *3*, 1832.
(26) Badenes, M. P.; Croce, A. E.; Cobos, C. J. *Phys. Chem. Chem. Phys.* **2004**, *6*, 747.
(27) Maricq, M. M.; Szente, J. J.; Li, Z.; Francisco, J. S. *J. Chem. Phys.* **1993**, *98*, 784.
(28) Maricq, M. M.; Szente, J. J.; Su, Y.; Francisco, J. S. *J. Chem. Phys.* **1994**, *100*, 8673.
(29) Arnold, D. W.; Bradforth, S. E.; Kim, E. H.; Neumark, D. M. *J. Chem. Phys.* **1995**, *102*, 3493.
(30) Argüello, G. A.; Grothe, H.; Kronberg, M.; Willner, H.; Mack, H.-G. *J. Phys. Chem.* **1995**, *99*, 17525.
(31) Williams, B. A.; Fleming, J. W. *J. Chem. Phys.* **1997**, *106*, 4376.
(32) Howie, W. H.; Lane, I. C.; Orr-Ewing, *J. Chem. Phys.* **2000**, *113*, 7237.
(33) Habara, H.; Yamamoto, S. *J. Mol. Spectrosc.* **2001**, *207*, 238,
(34) Zelinger, Z.; Dréan, P.; Walters, A.; Avilès Moreno, J. R.; Bogey, M.; Pernice, H.; vonAhsen, S.; Willner, H.; Breidung, J.; Thiel, W.; Bürger, H. *J. Chem. Phys.* **2003**, *118*, 1214.
(35) Francisco, J. S.; *Chem. Phys. Lett.* **1989**, *163*, 375.
(36) Francisco, J. S.; Goldstein, A. N.; Li, Z.; Zhao, Y. *J. Phys. Chem.* **1990**, *94*, 4791.
(37) Francisco, J. S.; Godstein, A. N.; Robb, M. A.; Williams, I. H. *Chem. Phys. Lett.* **1992**, *191*, 13.
(38) Zhao, Y.; Francisco, J. S. *Chem. Phys. Lett.* **1992**, *199*, 65.
(39) Krossner, Th.; Vetter, R.; Zülicke, L.; Peyerimhoff, S. D. *Chem. Phys. Lett.* **1992**, *193*, 236.
(40) Dibble, T.; Francisco, J. S. *J. Phys. Chem.* **1994**, *98*, 11694.
(41) Krossner, Th.; Zülicke, L.; Vetter, R.; Perić, M.; Peyerimhoff, S. D. *J. Chem. Phys.* **1994**, *101*, 3973
(42) Nanbu, S.; Gomyo, M.; Iwata, S. *Chem. Phys. Lett.* **1994**, *184*, 97.
(43) Schneider, W. F.; Maricq, M. M.; Francisco, J. S. *J. Chem. Phys.* **1995**, *103*, 6601.
(44) Staikova, M.; Peyerimhoff, S. D.; Zülicke, L. *J. Mol. Spectrosc*. **1995**, *170*, 356.
(45) Krossner, Th.; Perić, M.; Vetter, R.; Zülicke, L. *J. Chem. Phys.* **1994**, *101*, 3981. 236.
(46) Francisco, J. S.; Matti Mariq, M. In *Advances in Photochemistry*; Neckers, D. C., Volman, D. H., von Bünau, G., Eds.; John Wiley & Sons: New York, 1995; Vol. 20, p 79.
(47) Appelman, E. H.; Clyne, M. A. *J. Chem. Soc., Faraday Trans. 1* **1975**, *71*, 2072.
(48) Arvia, A. J.; Aymonino, P. J.; Waldow, C. H.; Schumacher, H. J. *Angew. Chem.* **1960**, *72*, 169.
(49) Arvia, A. J.; Aymonino, P. J.; Schumacher, H. J. *Z. Anorg. Allg. Chem.* **1962**, *316*, 327.
(50) Argüello, G. A.; Balzer-Jöllenbeck, G.; Jülicher, B.; Willner, H. *Inorg. Chem.* **1995**, *34*, 603.
(51) Timakov, A. A.; Prusakov, V. N. *Kinet. Katal.* **1989**, *30*, 472.
(52) Vasini, E. J..; Schumacher, H. J. *Z. Phys. Chem. NF*, **1968**, *65*, 238.
(53) Dicelio, L.; Schumacher, H. J. *An. Asoc. Quím. Argent.* **1978**, *66*, 283.
(54) Schack, C. J.; Christe, K. O. *Inorg. Nucl. Chem. Lett.* **1978**, *14*, 293.
(55) López, M. I.; Croce, A. E.; Sicre, J. E. *J. Photochem. Photobiol. A: Chem.* **1998**, *112*, 97.
(56) Fockenberg, C.; Somnitz, H.; Bednarek, G.; Zellner, R. *Ber. Bunsen-Ges. Phys. Chem.* **1997**, *101*, 1411.
(57) Tucceri, M. E.; Castellano, E.; Croce, A. E.; Cobos, C. J. *J. Arg. Chem. Soc.*, in press.
(58) Troe, J. *J. Phys. Chem.* **1979**, *83*, 114.
(59) Troe, J. *J. Chem. Phys.* **1977**, *66*, 4758.
(60) Troe, J. *Chem. Rev.* **2003**, *103*, 4565.
(61) Troe, J.; Ushakov, V. G. *Faraday Discuss. Chem. Soc.* **2001**, *119*, 145.
(62) Troe, J. *Int. J. Chem. Kinet.* **2001**, *33*, 878.
(63) Cobos, C. J.; Troe, J. *Z. Phys. Chem.* **2003**, *217*, 1031.
(64) Olzmann, M.; Troe, J. *Ber. Bunsen-Ges. Phys. Chem.* **1992**, *96*, 1327.
(65) Maergoiz, A. I.; Nikitin, E. E.; Troe, J.; Ushakov, V. G. *J. Chem. Phys.* **2002**, *117*, 4201.
(66) Hippler, H.; Troe, J.; Wendelken, H. J. *J. Chem. Phys.* **1983**, *78*, 6709.
(67) Reid, R. C.; Prausnitz, J. M.; Sherwood, T. K. *The Properties of Gases and Liquids*, 3rd ed.; MacGraw-Hill: New York, 1977.
(68) Croce de Cobos, A. E.; Cobos, C. J.; Castellano, E. *J. Phys. Chem.* **1989**, *93*, 274.
(69) Becke, A. D. *J. Chem. Phys.* **1983**, *98*, 5648.
(70) Becke, A. D. *Phys. Rev. A* **1988**, *38*, 3098.
(71) Lee, C.; Yang, W.; Parr, R. G. *Phys. Rev. B* **1988**, *37*, 785.
(72) Argüello, G. A.; Jülicher, B.; Ulic, S. E.; Willner, H.; Casper, B.; Mack, H.-G.; Oberhammer, H. *Inorg. Chem.* **1995**, *34*, 2089.
(73) Baboul, A. G.; Curtiss, L. A.; Redfern, P. C.; Raghavachari, K. *J. Chem. Phys.* **1999**, *110*, 7650.
(74) Sicre, J. E.; Cobos, C. J. *J. Mol. Struct. (THEOCHEM)* **2003**, *620*, 215.
(75) Chase, M., Jr. W.*NIST-JANAF Thermochemical Tables*, 4th ed. *J. Phys. Chem. Ref. Data* **1998**, Monograph No. 9.
(76) Curtiss, L. A.; Redfern, P. C.; Frurip, D. J. In *Reviews in Computational Chemistry*; Lipkowitz, K. B., Boyd, D. B., Eds.; Wiley-VCH: New York, 2000; Vol. 15, p 147.
(77) Hehre, W. J.; Radom, L.; Schleyer, P. v. R.; Pople, J. A. *Ab Initio Molecular Orbital Theory*; Wiley: New York, 1986.
(78) Curtiss, L. A.; Raghavachari, K.; Redfern, P. C.; Pople, J. A. *J. Chem. Phys.* **2000**, *112*, 1125.
(79) Frisch, M. J.; Trucks, G. W.; Schlegel, H. B.; Scuseria, G. E.; Robb, M. A.; Cheeseman, J. R.; Montgomery, J. A, Jr..; Vreven, T.; Kudin, K. N.; Burant, J. C.; Millam, J. M.; Iyengar, S. S.; Tomasi, J.; Barone, V.; Mennucci, B.; Cossi, M.; Scalmani, G.; Rega, N.; Petersson, G. A.; Nakatsuji, H.; Hada, M.; Ehara, M.; Toyota, K.; Fukuda, R.; Hasegawa, J.; Ishida, M.; Nakajima, T.; Honda, Y.; Kitao, O.; Nakai, H.; Klene, M.; Li, X.; Knox, J. E.; Hratchian, H. P.; Cross, J. B.; Adamo, C.; Jaramillo, J.; Gomperts, R.; Stratmann, R. E.; Yazyev, O.; Austin, A. J.; Cammi, R.; Pomelli, C.; Ochterski, J. W.; Ayala, P. Y.; Morokuma, K.; Voth, G. A.; Salvador, P.; Dannenberg, J. J.; Zakrzewski, V. G.; Dapprich, S.; Daniels, A. D.; Strain, M. C.; Farkas, O.; Malick, D. K.; Rabuck, A. D.; Raghavachari, K.; Foresman, J. B.; Ortiz, J. V.; Cui, Q.; Baboul, A. G.; Clifford, S.; Cioslowski, J.; Stefanov, B. B.; Liu, G.; Liashenko, A.; Piskorz, P.; Komaromi, I.; Martin, R. L.; Fox, D. J.; Keith, T.; Al-Laham, M. A.; Peng, C. Y.; Nanayakkara, A.; Challacombe, M.; Gill, P. M. W.; Johnson, B.; Chen, W.; Wong, M. W.; Gonzalez, C.; Pople, J. A. *Gaussian 03*, revision C.02; Gaussian, Inc.: Pittsburgh, PA, 2004.
(80) Troe, J. *J. Chem. Phys.* **1977**, *66*, 4745.
(81) Hippler, H.; Troe, J. In *Bimolecular Collisions*; Ashfold, M. N. R., Baggott, J. E., Eds.; Advances in Gas-Phase Photochemistry and Kinetics; Royal Society of Chemistry: London, 1989; p 209 (see also references therein).
(82) Troe, J. *J. Chem. Phys.* **1981**, *75*, 226.
(83) Cobos, C. J.; Troe, J. *J. Chem. Phys.* **1985**, *83*, 1010.
(84) Nikitin, E. E. *Theor. Exp. Chem.* **1965**, *1*, 144.
(85) Pechukas, P.; Light, J. C. *J. Chem. Phys.* **1965**, *42*, 3281.
(86) Maergoiz, A. I.; Nikitin, E. E.; Troe, J.; Ushakov, V. G. *J. Chem. Phys.* **1998**, *108*, 5265.